

Frequency upconversion in rare-earth doped fluoroindate glasses

Cid B. de Araújo^{a*}, Glauco S. Maciel^a, Leonardo de S. Menezes^a, Nikifor Rakov^a, Edilson L. Falcão-Filho^a, Vladimir A. Jerez^a, Younes Messaddeq^b

^a Departamento de Física, Universidade Federal de Pernambuco, 50670-901 Recife, PE, Brazil

^b Instituto de Química, Universidade do Estado de São Paulo, 14801-970, Araraquara, SP, Brazil

Received 21 May 2002; accepted 26 June 2002

Abstract – We present recent results on frequency upconversion (UPC) obtained in fluoroindate glasses (FIG) doped with Ho³⁺, Tm³⁺ and Nd³⁺ ions and codoped with Pr³⁺/Nd³⁺ and Yb³⁺/Tb³⁺ ions. The results for the Ho³⁺-doped samples show strong evidence of energy transfer (ET) between Ho³⁺ ions resonantly excited at 640 nm. The origin of the blue-green upconverted fluorescence observed was identified and the dynamics of the signals revealed the pathways involved in the UPC process. In the case of Tm³⁺-doped FIG, the samples were resonantly excited at 650 nm and the main mechanism that contributes for the red-to-blue upconversion is excited-state absorption (ESA). The FIG samples codoped with Pr³⁺/Nd³⁺ were excited at 588 nm in resonance with transitions starting from the ground state of the Nd³⁺ and the Pr³⁺ ions. It was observed that the presence of Nd³⁺ ions enhanced the Pr³⁺ emission at 480 nm by two orders of magnitude. Multiphonon (MP)-assisted upconversion is also discussed for Nd³⁺-doped FIG pumped at 866 nm. Emission at 750 nm with a peculiar linear dependence with the laser intensity was observed and explained. A rate-equation model that includes MP absorption via thermally coupled electronic excited states of Nd³⁺ was developed and describes well the experimental results. The role played by effective phonon modes is clearly demonstrated. MP-assisted UPC process was also studied in Yb³⁺/Tb³⁺-codoped FIG samples excited at 1064 nm, which is off-resonance with electronic transitions starting from the ground state. It was determined that the mechanism leading to Tb³⁺ emission in the blue is due to ET from a pair of excited Yb³⁺ ions followed by ESA in the Tb³⁺ ions. **To cite this article:** Cid B. de Araújo et al., C. R. Chimie 5 (2002) 885–898 © 2002 Académie des sciences/Éditions scientifiques et médicales Elsevier SAS

frequency upconversion / fluoroindate glass / rare-earth ions

Résumé – Des résultats récents relatifs à la conversion ascendante de fréquence dans le verre fluoroindate (FIG) dopé avec ions Ho³⁺, Tm³⁺ et Nd³⁺ ou codopé avec Pr³⁺/Nd³⁺ et Yb³⁺/Tb³⁺ sont présentés. Les expériences réalisées sur Ho³⁺ mettent clairement en évidence un transfert d'énergie entre les ions Ho³⁺ excités à la longueur d'onde 640 nm. L'origine des fluorescences bleue et verte a été identifiée ; la dynamique des signaux permet de mettre en évidence les chemins d'excitation dans les processus de conversion ascendants. Les échantillons contenant Tm³⁺ étaient excités par un laser émettant à 650 nm : le processus dominant pour la conversion ascendante rouge-bleu est l'absorption, pour les états excités d'un même ion. Les verres codopés Pr³⁺/Nd³⁺ étaient excités à 588 nm. La présence du Nd³⁺ a augmenté l'émission à 480 nm par le Pr³⁺ de deux ordres de grandeur. L'émission visible assistée par un processus de multiphonons est présentée pour Nd³⁺ pompé à 866 nm. Une émission à 750 nm avec dépendance linéaire en puissance de pompage a aussi été observée et expliquée. Un modèle faisant intervenir une équation incluant l'absorption multiphonon via un couplage thermique entre états excités du Nd³⁺ rend bien compte des résultats expérimentaux. Les processus assistés par phonons ont aussi été étudiés en ce qui concerne le codopage Yb³⁺/Tb³⁺. On a déterminé que l'émission du Tb³⁺ dans le bleu est liée au transfert de l'énergie accumulée dans deux ions Yb³⁺ voisins à des niveaux excités du Tb³⁺. **Pour citer cet article :** Cid B. de Araújo et al., C. R. Chimie 5 (2002) 885–898 © 2002 Académie des sciences/Éditions scientifiques et médicales Elsevier SAS

conversion ascendante de fréquence / verre fluoroindate / terre rare

* Corresponding author.

E-mail address: cid@df.ufpe.br (C.B. de Araújo).

1. Introduction

The discovery of fluorindate glasses (FIG) is not recent [1, 2]. However, along the past 15 years, a number of improvements in their characteristics were developed. Presently, these compounds are prepared with very good optical quality; they are very stable against atmospheric moisture, present a low refractive index and low optical attenuation from the ultraviolet to the middle infrared. Nowadays, optical fibers can be prepared [3] and a number of applications have been considered. Different methods can be used to prepare planar waveguides in FIG substrates [4–6].

Numerous publications on the physical properties of FIG have been dedicated to the study of the optical absorption characteristics of FIG in the visible and in the infrared, as well as to the investigation of Raman scattering properties (see for example [7–11] and references therein). Many publications related to the chemical properties of FIG such as the method of preparation [12–14], morphology [14, 15], devitrification kinetics [16], stabilization [14–17] and thermal properties [6, 18, 19] are available. As the phonon cut-off energy of the FIG matrix is small ($\sim 507\text{ cm}^{-1}$) [7], multiphonon emission rates between close electronic levels of rare earth (RE) ions in FIG are feeble.

The phenomenon of frequency upconversion (UPC), a process in which high-frequency photons are emitted after excitation of the sample by low energy photons, has also been studied in RE doped FIG [11, 20–39]. We have studied UPC in FIG doped with Pr^{3+} [31], Er^{3+} [32, 33], Nd^{3+} [34, 35], Ho^{3+} [36], $\text{Yb}^{3+}/\text{Pr}^{3+}$ [37], and $\text{Yb}^{3+}/\text{Tb}^{3+}$ [38]. The results demonstrate the large potential of FIG for photonic applications such as upconverters, lasers, optical amplifiers and thermal sensors. For example, we have demonstrated the potential of Nd^{3+} -doped FIG for blue lasing [39], and Er^{3+} -doped FIG for temperature sensing [40] and optical modulation [41]. Other authors demonstrate the use of FIG as laser host [42, 43].

In this article we review our recent studies on UPC in fluorindate glasses doped with Ho^{3+} and Nd^{3+}

ions, as well as present new results for FIG doped with Tm^{3+} and codoped with $\text{Pr}^{3+}/\text{Nd}^{3+}$ and $\text{Yb}^{3+}/\text{Tb}^{3+}$.

2. Experimental details

The samples used have the compositions indicated in Table 1. The glass synthesis was made using standard pro-analysis oxides and fluorides as starting materials. The fluoride powders used to prepare the desired compositions were mixed together and heat-treated first at $700\text{ }^\circ\text{C}$ for melting and then $800\text{ }^\circ\text{C}$ for refining. The melt was finally poured between two preheated brass plates to allow the preparation of samples of different thicknesses. Fining, casting and annealing were carried out in a way similar to standard fluoride glasses under a dry argon atmosphere. Non-hygroscopic samples are obtained with a very good optical quality.

Optical absorption measurements in the range $0.2\text{--}1.2\text{ }\mu\text{m}$ were made using a diode-array spectrophotometer. For all measurements, the spectrophotometer bandwidth was smaller than the linewidths of the absorption bands, which are mainly due to inhomogeneous broadening of the electronic transitions. The optical absorption spectra of the FIG samples studied here are shown in Fig. 1. The absorption bands were identified by comparison with other RE trivalent ions doped glasses and crystal systems [44, 45], since the energy levels of RE trivalent ions do not change significantly for different hosts.

The experimental apparatus used in the UPC experiments is described in Section 4.

3. Theoretical background

The absorption bands observed from the near-ultraviolet to the near-infrared spectra of RE doped glasses are usually due to $4f\text{--}4f$ transitions. In this work, they are associated to induced electric dipole

Table 1. Molar composition (in %) of the fluorindate glasses studied.

Sample	InF_3	ZnF_2	SrF_2	BaF_2	NaF	GaF_3	GdF_3	HoF_3	NdF_3	TmF_3	PrF_3	TbF_3	YbF_3
Ho5	38	20	20	15.5	2.0	4.0	—	0.5	—	—	—	—	—
Ho10	38	20	20	15	2.0	4.0	—	1.0	—	—	—	—	—
Ho20	38	20	20	14	2.0	4.0	—	2.0	—	—	—	—	—
Tm10	38	20	20	16	2.0	2.0	2.0	—	—	1.0	—	—	—
Tm20	37	20	20	16	2.0	2.0	2.0	—	—	2.0	—	—	—
Tm30	36	20	20	16	2.0	2.0	2.0	—	—	3.0	—	—	—
Nd10	38	20	20	16	2.0	2.0	1.0	—	1.0	—	—	—	—
Pr2Nd1	38	20	20	15.7	2.0	4.0	—	—	0.1	—	0.2	—	—
Pr2Nd2	38	20	20	15.6	2.0	4.0	—	—	0.2	—	0.2	—	—
Yb15Tb	37.5	20	20	14.5	2.0	4.0	—	—	—	—	—	0.5	1.5
Yb20Tb	37	20	20	14.5	2.0	4.0	—	—	—	—	—	0.5	2.0

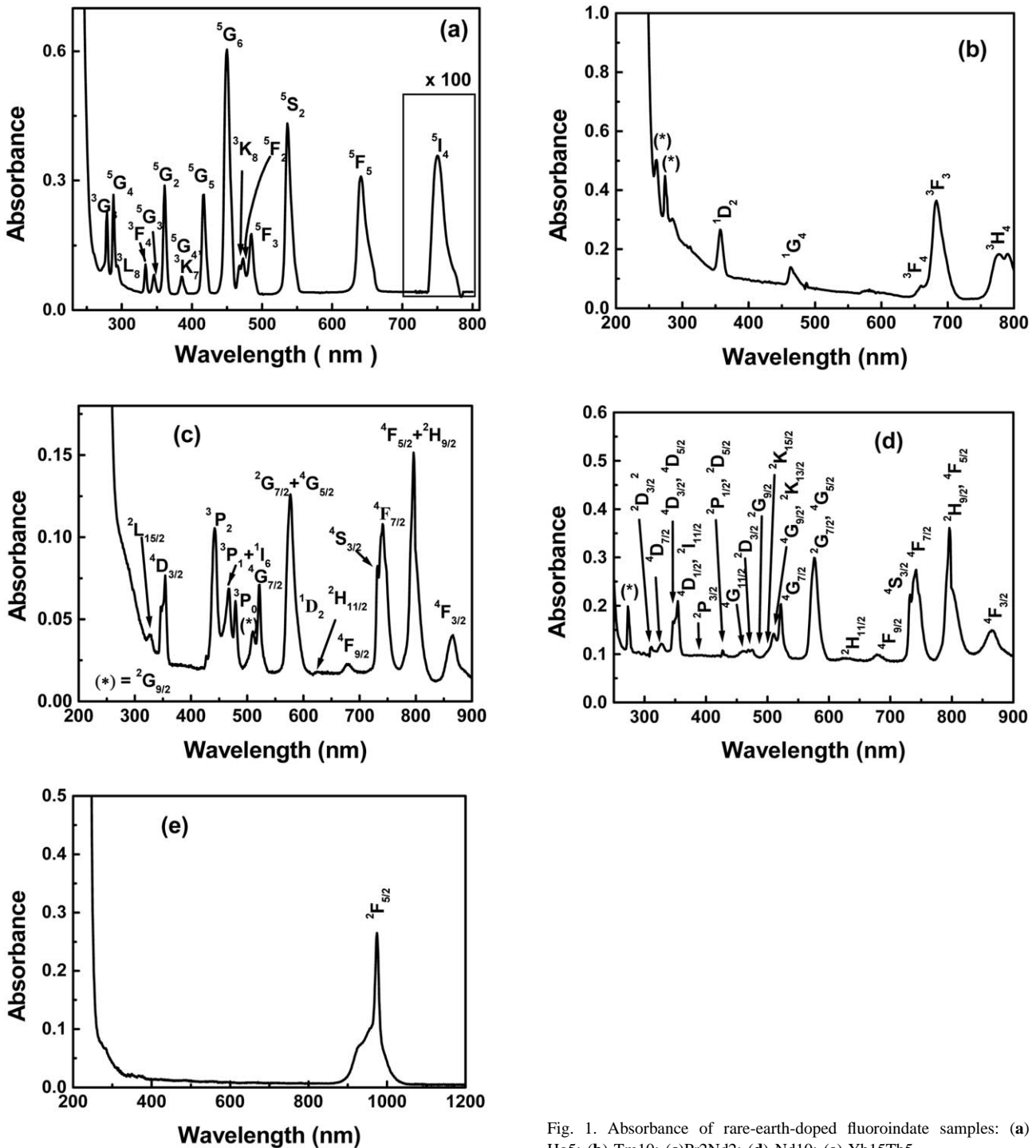


Fig. 1. Absorbance of rare-earth-doped fluoroindate samples: (a) Ho5; (b) Tm10; (c) Pr2Nd2; (d) Nd10; (e) Yb15Tb5.

transitions. The dipole strength of a transition, written in esu units, can be expressed as [45]:

$$P = \frac{2303 m c^2}{N \pi e^2} \int \epsilon_i(\nu) d\nu \quad (1)$$

where m is the electron mass, c is the speed of light, N is the Avogadro number, e is the electron charge and $\epsilon(\nu)$ is the molar absorptivity of a band with

energy ν (in cm^{-1}), which is computed from the Beer–Lambert law. On the other hand, the value of P between two multiplets J and J' can be calculated using the Judd–Ofelt (JO) theory [46, 47] and is given by:

$$P = \frac{8 \pi^2 m c \sigma}{3 h (2J + 1)} \chi_a \sum_{\lambda=2,4,6} \Omega_\lambda |\langle aJ' \| U^{(\lambda)} \| bJ \rangle|^2 \quad (2)$$

where σ is the mean energy between the two multiplets (in cm^{-1}), $\chi_a = (n^2 + 2)^2/9n$ is the Lorentz local field correction for the absorption, n is the refractive index of the medium, $U^{(\lambda)}$ ($\lambda = 1, 2, 3$) are unit operators of rank λ and W_λ are the JO intensity parameters.

Equation (1) allows us to obtain the P value for each transition; these values can be used in equation (2) to determine the JO parameters. The probability of spontaneous radiative emission between J and J' levels is given by:

$$A_{JJ'} = \frac{64 \pi^4 \sigma^3}{3 h (2J + 1)} \chi_e S_{\text{ed}} \quad (3)$$

where $\chi_e = n(n^2 + 2)^2/9$ is the effective field correction for emission at a well-localized center in a medium of isotropic refractive index n . S_{ed} is the electric dipole line strength defined as:

$$S_{\text{ed}} = e^2 \sum_{\lambda=2,4,6} \Omega_\lambda |\langle aJ' \| U^{(\lambda)} \| bJ \rangle|^2 \quad (4)$$

The radiative lifetime of an excited state is calculated by $\tau_R = (\sum_{J'} A_{JJ'})^{-1}$ and the branching ratio corresponding to the emission from an excited level J to J' is given by $\beta_{JJ'} = A_{JJ'} \tau_R$.

Another important parameter concerning the luminescence intensity produced by a given RE ion is the quantum efficiency, defined as the ratio between the measured lifetime (τ_m) of an excited state and its radiative lifetime. The value of τ_m corresponds to $(\tau_R^{-1} + W_{\text{NR}})^{-1}$, where W_{NR} represents the nonradiative decay rate [44, 45]. W_{NR} contains the probability that an excited RE ion decays nonradiatively delivering its energy to the host lattice or to another RE ion. The energy delivered to the host originates phonons and therefore the sample's temperature increases. The non-radiative relaxation channel competes with the radiative one and therefore the emission of photons by RE ions may be quenched in solids due to phonons of the host material or to energy transfer (ET) to another ion. A good upconverter material is one that has large luminescence quantum efficiency, i.e., a low nonradiative emission probability. Assuming weak interaction between RE ions, this is accomplished when the cut-off phonon energy of the host is small. Accordingly, silicate glass with phonon cut-off energy of $\sim 1100 \text{ cm}^{-1}$ presents a lower luminescence efficiency than FIG that present a phonon cut-off energy of $\sim 507 \text{ cm}^{-1}$ [7].

4. Results and discussion

In this section, our UPC experiments in RE-doped FIG are discussed. The dynamics of UPC fluorescence is analyzed and its temperature dependence investi-

gated. The UPC measurements in the Ho^{3+} , Tm^{3+} , and $\text{Pr}^{3+}/\text{Nd}^{3+}$ doped samples were performed using dye lasers pumped by the second harmonic of a Q-switched Nd:YAG laser (532 nm, 15 ns, 5 Hz). The measurements in the Nd^{3+} -doped sample were made using a CW Ti:Sapphire laser (866 nm). For the samples codoped with Yb^{3+} and Tb^{3+} , we used a mode-locked (76 MHz) Nd:YAG laser operating at 1064 nm. The upconverted fluorescence in the dye laser experiments was collected along a direction perpendicular to the incident beam and it was dispersed by a 0.25-m spectrometer, being detected by a photomultiplier and sent to a digital oscilloscope. The average of many successive scans was recorded by a computer. In the CW experiments, the signal, also collected in the perpendicular direction to the laser beam, was sent to a lock-in amplifier before being recorded by a computer. The measurements in the Ho^{3+} -, Tm^{3+} -, and $\text{Pr}^{3+}/\text{Nd}^{3+}$ -doped samples were performed at room temperature. The Nd^{3+} - and $\text{Yb}^{3+}/\text{Tb}^{3+}$ -doped samples were contained in an oven, whose temperature was adjusted from room temperature to 500 K.

4.1. UPC dynamics

4.1.1. Ho^{3+} -doped FIG

The optical properties of Ho^{3+} -doped glasses and crystals have been studied aiming to the operation of UPC lasers [48, 49]. Blue-green UPC luminescence owing to 4f-4f transitions of Ho^{3+} has been observed upon visible and infrared excitation, with efficiencies that are highly dependent on the host matrix [50, 51], demonstrating the importance of studying UPC processes in new materials.

In this section, we discuss the UPC phenomenon in Ho^{3+} -doped FIG excited by a nanosecond laser operating at 640 nm. Green and blue anti-Stokes emissions owing to ET mechanisms were observed and the analysis of the results allowed us to identify the pathways that contribute to the UPC emissions.

The absorption spectrum of sample Ho5 is shown in Fig. 1a. No changes were observed in the lineshape or in the peak positions corresponding to the various transitions, for different Ho^{3+} concentrations. The method of spectral-band intensity analysis [52] was used to estimate the JO parameters of our samples; the values are presented in Table 2.

The UPC spectrum is shown in Fig. 2 for excitation at 640 nm, in resonance with the transition $^5\text{I}_8 \rightarrow ^5\text{F}_5$. Fig. 2a shows two bands centered at $\sim 550 \text{ nm}$ and $\sim 490 \text{ nm}$ due to transitions $^5\text{S}_2 \rightarrow ^5\text{I}_8$ and $^5\text{F}_3 \rightarrow ^5\text{I}_8$, respectively, while Fig. 2b shows bands centered at $\sim 395 \text{ nm}$ and $\sim 425 \text{ nm}$ corresponding to transitions $(^3\text{K}_7, ^5\text{G}_4) \rightarrow ^5\text{I}_8$ and $^5\text{G}_5 \rightarrow ^5\text{I}_8$, respectively. The inten-

Table 2. Spontaneous emission probabilities of relevant Ho³⁺ excited states in fluoroindate glass.

Energy level	A_r (s ⁻¹)	τ_r (ms)	A_{nr} (s ⁻¹)
⁵ F ₅	2.15×10^3	0.5	3×10^4
⁵ S ₂	2.54×10^3	0.4	1×10^3
⁵ F ₃	5.47×10^3	0.2	2×10^5
⁵ G ₄ , ³ K ₇	4.67×10^3	0.2	6×10^5
⁵ G ₅	5.50×10^3	0.2	6×10^5

 Table 3. Dynamics of the upconversion signal of Ho³⁺-doped fluoroindate glasses. Estimated data error: 5%.

[Ho ³⁺] (mol%)	0.5	1	2
Rise time @ 548 nm	3.6 μ s	4.2 μ s	3.2 μ s
Decay time @ 548 nm	116 μ s	78 μ s	48 μ s
Rise time @ 490 nm	0.4 μ s	0.4 μ s	0.4 μ s
Decay time (1) @ 490 nm	3 μ s	3 μ s	3 μ s
Decay time (2) @ 490 nm	22 μ s	20 μ s	18 μ s

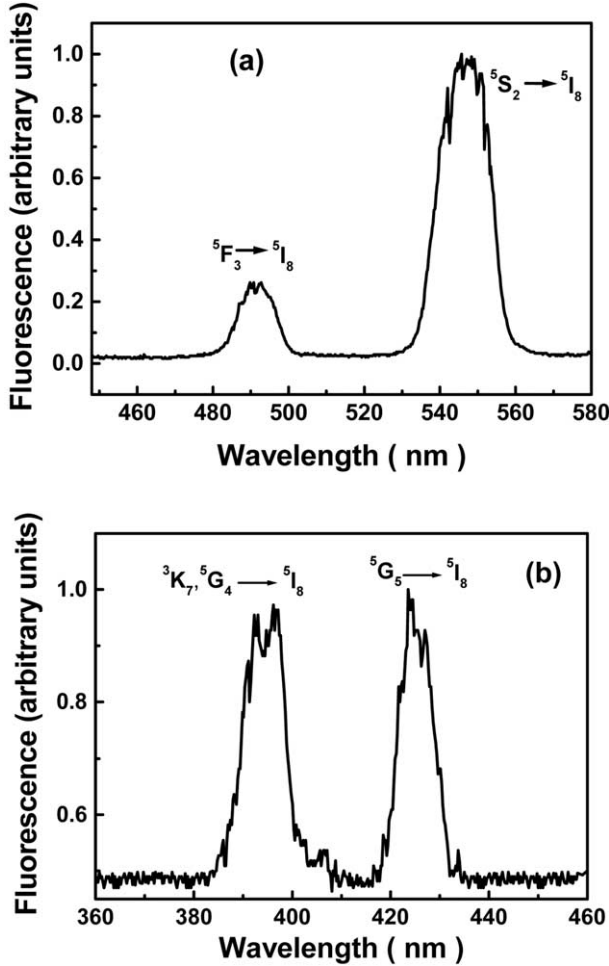


Fig. 2. Upconversion spectrum of sample Ho5 for excitation at 640 nm. The intensity of the bands shown in (a) are two orders of magnitude larger than in (b).

sities of the bands shown in Fig. 2b are two orders of magnitude weaker than those shown in Fig. 2a.

The green luminescence at ~550 nm presented a rise time between 3.2 and 4.2 μ s, and a decay time that changes more than 50% (116 to 48 μ s) for the range of Ho³⁺ concentrations investigated here. The blue emission at ~490 nm presented a rise time that is shorter than the green signal rise time and shows a double exponential decay. The longer decay time component of the blue emission (22 to 18 μ s) is depen-

dent on the Ho³⁺ concentration. The results are summarized in Table 3. The dependence of the UPC signal as a function of pump intensity and Ho³⁺ concentration were also investigated. A quadratic dependence was observed in both experiments indicating that two laser photons are absorbed to originate each UPC photon and a pair of Ho³⁺ ions are involved in the UPC process. The emissions at ~380 nm and ~440 nm are very weak and it was not possible to analyze their temporal behavior. It is important to note that these emissions have not been observed in other glass hosts [53], probably because their intensities were strongly reduced, due to nonradiative relaxation.

Fig. 3 shows the energy level diagram of Ho³⁺ and the main pathways responsible for the UPC processes. We expect that the UPC emission is due to ET between two ions at level ⁵F₅, which are directly excited by laser photons at 640 nm. The lifetime of level ⁵F₅ is large enough to allow significant ET between excited ions and two possible channels may populate level ⁵F₃ via ET. One channel is an indirect ET assisted UPC (ETAU) via ⁵F₅ + ⁵F₅ → ⁵I₇ + (³K₇, ⁵G₄), with subsequent population decay to level ⁵F₃ via multiphonon emission from levels ⁵G₄ and ³K₇. The other channel is related to a direct ETAU via ⁵F₅ + ⁵F₅ → ⁵I₅ + ⁵F₃. We observed that the intensity of the UPC signal shows a quadratic dependence with Ho³⁺ concentration, which indicates that pair interaction is a relevant process.

Using a rate equations approach to describe the UPC process, it is possible to estimate the ET rates from level ⁵F₅ to level ⁵F₃ considering the following equations:

$$dN_d/dt = -2 \gamma_1 N_d - (W_{12} + W_{13}) N_d \quad (6)$$

$$dn_2/dt = -\gamma_2 n_2 + \gamma_{32} n_3 + W_{12} N_d \quad (7)$$

$$dn_3/dt = -\gamma_3 n_3 + W_{13} N_d \quad (8)$$

N_d represents the population density belonging to a pair of excited ions at level ⁵F₅ (the factor 2 in equation (6) arises because an excited pair is annihilated as soon as one of the ions de-excites); $(\gamma_1)^{-1}$ is the lifetime of level ⁵F₅, n_2 and n_3 stand for the

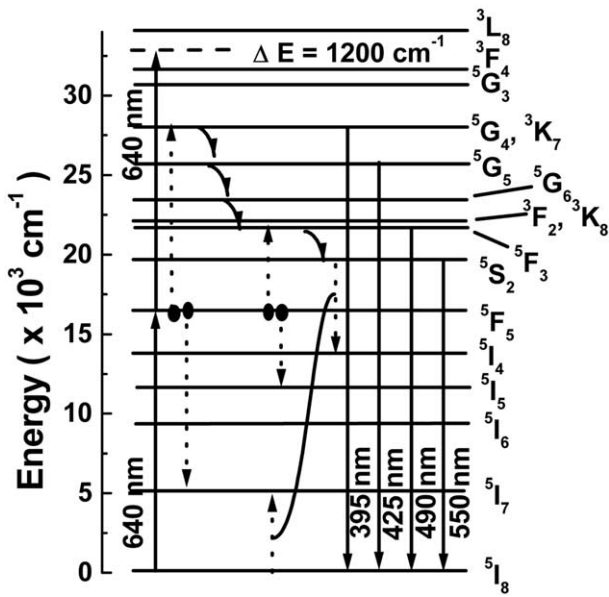


Fig. 3. Energy-level scheme of Ho^{3+} . Solid lines indicate radiative transitions; curved arrows represent phonon relaxations; dashed lines refer to energy transfer processes.

population densities of level ${}^5\text{F}_3$ and level (${}^3\text{K}_7$, ${}^5\text{G}_4$), respectively. The parameters $(\gamma_2)^{-1}$ and $(\gamma_3)^{-1}$ are the lifetimes of level ${}^5\text{F}_3$ and levels (${}^3\text{K}_7$, ${}^5\text{G}_4$), respectively. γ_{32} is the multi-step nonradiative decay rate from level (${}^3\text{K}_7$, ${}^5\text{G}_4$) to level ${}^5\text{F}_3$, and W_{ij} ($i, j = 1, 2, 3$) are cross-relaxation rates. The dynamics of the population at level ${}^5\text{F}_3$ is understood by solving the system of equations (6) to (8) and the solution is given by

$$n_2(t) = A e^{-(2\gamma_1 + W_{12} + W_{13})t} - B e^{-\gamma_3 t} + C e^{-\gamma_2 t}$$

where A , B and C are given in terms of the relaxation parameters.

The fluorescence intensity at ~ 490 nm is proportional to $n_2(t)$ and, from the data shown in Table 3, we associate γ_2 to the short-decay time component and therefore it is related to level ${}^5\text{F}_3$ lifetime (estimated ca $5 \mu\text{s}$ from Table 2). The value of $(\gamma_3)^{-1}$ is dominated by $(\gamma_{32})^{-1} \sim 0.6 \mu\text{s}$, while the lifetime of ${}^5\text{F}_5$ is $\sim 47 \mu\text{s}$. The Stokes shifted emission at 653 nm (transition ${}^5\text{F}_5 \rightarrow {}^5\text{I}_8$) was used to evaluate the lifetime of level ${}^5\text{F}_5$ using the less concentrated sample available with low excitation power at 640 nm. The signal decay was fitted with a single exponential curve yielding $\sim 47 \mu\text{s}$ of decay time. Therefore $(\gamma_3)^{-1}$ is associated to the rise time of the blue luminescence while $(2\gamma_1 + W_{12} + W_{13})^{-1}$ is associated with the decay time. The cross-relaxation rates found are shown in Table 4. The measured rise time ($0.4 \mu\text{s}$), shorter than the value estimated via multiphonon emission rates from level (${}^3\text{K}_7$, ${}^5\text{G}_4$), may be due to the fact that the signal centered at ~ 490 nm has a contribution from

Table 4. Energy-transfer rates estimated from the experimental data.

$[\text{Ho}^{3+}]$ mol%	0.5	1	2
$W_{12} + W_{13}$ (s^{-1})	3×10^3	7×10^3	13×10^3
W_R (s^{-1})	6×10^3	10×10^3	18×10^3

excited pairs decaying coherently (simultaneously) to lower-lying energy levels on a faster timescale than those pairs decaying incoherently. Values for A , B and C were obtained fitting the expression for $n_2(t)$ to the experimental data for the intensity decay.

To understand the behavior of the emission at ~ 550 nm, we assume that the population at level ${}^5\text{S}_2$ is loaded via level ${}^5\text{F}_3$, because the rise time of the green fluorescence has the same order of magnitude as the lifetime of state ${}^5\text{F}_3$, which is dominated by the nonradiative relaxation ${}^5\text{F}_3 \rightarrow {}^5\text{S}_2$ ($2 \times 10^5 \text{ s}^{-1}$). We recall that the green fluorescence decay time is dependent on the Ho^{3+} concentration, as indicated in Table 3. The cross-relaxation channel that depopulates level ${}^5\text{S}_2$ (${}^5\text{S}_2 + {}^5\text{I}_8 \rightarrow {}^5\text{I}_4 + {}^5\text{I}_7$) is efficient only after the cross-relaxation processes that lead to the blue luminescence takes place (see Fig. 3) [53]. Again, the rate equations approach is used to estimate the cross-relaxation rates from level ${}^5\text{S}_2$ through the following equations:

$$dn'_1/dt = -\gamma'_1 n'_1 \quad (9)$$

$$dn'_2/dt = \gamma'_1 n'_1 - (\gamma'_2 + W_R) n'_2 \quad (10)$$

Here, 1 corresponds to level ${}^5\text{F}_3$ and 2 is associated to level ${}^5\text{S}_2$. The parameter γ'_1 (γ'_2) is the decay rate of level ${}^5\text{F}_3$ (${}^5\text{S}_2$) and W_R is the cross-relaxation rate. The ground state population was assumed to be non-depleted and thus the solution of the rate equations system yielded a simple equation that governs the dynamics of the population at level ${}^5\text{S}_2$, given by $n'_2(t) = A e^{-\gamma'_1 t} - B e^{-(\gamma'_2 + W_R)t}$. The parameter $(\gamma'_1)^{-1}$ is the lifetime of level ${}^5\text{F}_3$ and $(\gamma'_2 + W_R)^{-1}$ corresponds to the quenched lifetime of level ${}^5\text{S}_2$. As the values of γ'_1 and γ'_2 are known, it is straightforward to find W_R from the data of Tables 2 and 3. The values found for W_R are shown in Table 4.

4.1.2. Tm^{3+} -doped FIG

Thulium (Tm^{3+}) is one of the most efficient rare-earth ions for obtaining laser emission, frequency upconversion, as well as to be used in optical amplifiers, when doping different hosts [44, 54, 55]. Frequency upconversion in a variety of Tm^{3+} doped materials has also been investigated [23, 56–62]. Of particular interest is the possibility of obtaining strong blue emission from Tm^{3+} doped materials pumped in the red and in the infrared. Upconversion laser emis-

Table 5. Oscillator strength values and intensity parameters of Tm^{3+} doped fluoroindate glasses.

Level	Energy (cm^{-1})	f_{exp}	f_{cal}
$^3\text{F}_4$	5920	1.79×10^{-06}	1.85×10^{-06}
$^3\text{H}_5$	8320	1.43×10^{-06}	1.29×10^{-06}
$^3\text{H}_4$	12 771	1.92×10^{-06}	1.94×10^{-06}
$^3\text{F}_{3,2}$	14 620	2.95×10^{-06}	2.98×10^{-06}
$^1\text{G}_4$	21 445	0.70×10^{-06}	0.56×10^{-06}
$^1\text{D}_2$	28 011	1.91×10^{-06}	1.90×10^{-06}
Ω_2	$2.36 \times 10^{-20} \text{ cm}^2$		
Ω_4	$1.59 \times 10^{-20} \text{ cm}^2$		
Ω_6	$1.21 \times 10^{-20} \text{ cm}^2$		

sion and amplified spontaneous emission studies have been reported for Tm^{3+} doped optical fibers [63, 64].

In this section we present spectroscopic properties of FIG samples doped with Tm^{3+} . Fig. 1b shows the absorption spectrum of one of the samples. The dynamics of the fluorescence was studied and a model for the UPC process is given. Rates of energy transfer between Tm^{3+} ions are also provided.

From the absorption spectra of the samples studied we calculated the JO parameters: $O_2 = 2.36 \times 10^{-20} \text{ cm}^2$, $O_4 = 1.59 \times 10^{-20} \text{ cm}^2$, and $O_6 = 1.21 \times 10^{-20} \text{ cm}^2$. Oscillator strengths, branching ratios, radiative lifetimes and multiphonon relaxation

rates were determined for all Tm^{3+} levels and the results are presented in Tables 5 and 6.

Fluorescence measurements were performed tuning the dye laser wavelength from 624 to 686 nm. Fig. 4 shows the emission spectrum of the sample Tm10 pumped at 650 nm, in resonance with transition $^3\text{H}_6 \rightarrow ^3\text{F}_2$. The band centered at $12\,625 \text{ cm}^{-1}$ corresponds to transition $^3\text{F}_4 \rightarrow ^3\text{H}_6$. The UPC emissions are associated to transitions $^1\text{D}_2 \rightarrow ^3\text{F}_4$ ($22\,220 \text{ cm}^{-1}$) and $^1\text{D}_2 \rightarrow ^3\text{H}_6$ ($27\,550 \text{ cm}^{-1}$). The emissions from state $^1\text{D}_2$ present a quadratic dependence with the laser intensity and the excitation spectrum of both UPC emissions show a peak at 658 nm. No UPC emission is observed when the laser is tuned to transition $^3\text{H}_6 \rightarrow ^3\text{F}_3$.

The time evolution of the fluorescence shows a non-exponential decay for the three samples studied indicating the contribution of ion–ion interactions. Signal risetimes in the range from 150 ns to 316 ns, depending on the Tm^{3+} concentration, were measured for transition $^3\text{H}_4 \rightarrow ^3\text{H}_6$ with decay times varying from 560 to 44 μs . The risetime of the UPC transitions follows the laser pulse, while the decay time decrease from 26 to 6 μs as the Tm^{3+} concentration increases. The identified UPC pathway is indicated in Fig. 5,

 Table 6. Radiative transition probability $A_{JJ'}$ (s^{-1}), radiative lifetime τ_{R} (μs), branching ratio $\beta_{JJ'}$ and multiphonon relaxation rate W_{MP} (s^{-1}) of Tm^{3+} -doped FIG.

Transition	Energy gap (cm^{-1})	$A_{JJ'}$	$\beta_{JJ'}$	$\beta_{JJ'} (\text{exp})$	τ_{R}	W_{MP}
$^3\text{F}_4 \rightarrow ^3\text{H}_6$	5920	140	1		7117	2.32×10^{-04}
$^3\text{H}_5 \rightarrow ^3\text{F}_4$	2400	4	0.025		6170	3.91×10^{04}
$^3\text{H}_6$	8320	157	0.975			5.69×10^{-10}
$^3\text{H}_4 \rightarrow ^3\text{H}_5$	4451	16	0.022		1251	6.28×10^{-01}
$^3\text{F}_4$	6851	59	0.074			1.54×10^{-06}
$^3\text{H}_6$	12 771	722	0.904			2.25×10^{-20}
$^3\text{F}_3 \rightarrow ^3\text{H}_4$	2006	2.7	0.002		576	3.26×10^{05}
$^3\text{H}_5$	6457	169	0.098			1.29×10^{-05}
$^3\text{F}_4$	8857	45	0.026			3.16×10^{-11}
$^3\text{H}_6$	14 777	1516	0.874			4.61×10^{-25}
$^3\text{F}_2 \rightarrow ^3\text{F}_3$	374	0.0	0.0		1143	2.12×10^{09}
$^3\text{H}_4$	2380	6.2	0.007			4.35×10^{04}
$^3\text{H}_5$	6831	112	0.128			1.72×10^{-06}
$^3\text{F}_4$	9231	291	0.333			4.23×10^{-12}
$^3\text{H}_6$	15 151	464	0.532			6.16×10^{-26}
$^1\text{G}_4 \rightarrow ^3\text{F}_2$	6294	10	0.008		791	3.10×10^{-05}
$^3\text{F}_3$	6680	34	0.028			3.88×10^{-06}
$^3\text{H}_4$	8674	128.2	0.102			8.47×10^{-11}
$^3\text{H}_5$	13 125	435.3	0.345			3.35×10^{-21}
$^3\text{F}_4$	15 525	105.3	0.083			8.23×10^{-27}
$^3\text{H}_6$	21 445	549.5	0.434			1.20×10^{-40}
$^1\text{D}_2 \rightarrow ^1\text{G}_4$	6566	77	0.005		67	7.16×10^{-06}
$^3\text{F}_2$	12 860	589	0.044			1.39×10^{-20}
$^3\text{F}_3$	13 234	499	0.034			1.86×10^{-21}
$^3\text{H}_4$	15 240	674	0.046			3.82×10^{-26}
$^3\text{H}_5$	19 691	38	0.003			1.51×10^{-36}
$^3\text{F}_4$	22 091	7031	0.477	0.544		3.71×10^{-42}
$^3\text{H}_6$	28 011	5836	0.396	0.350		5.40×10^{-56}

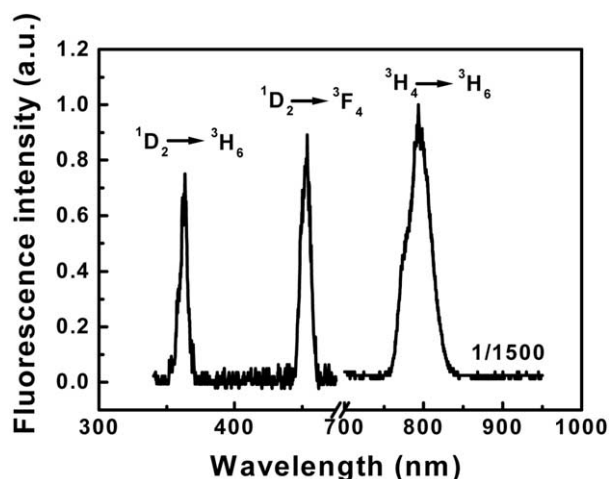


Fig. 4. Fluorescence spectrum of sample Tm10 pumped at 650 nm.

where the excited state absorption ${}^3\text{H}_4 \rightarrow {}^1\text{D}_2$ is indicated as the dominant process.

Interaction between Tm^{3+} ions, as revealed by the non-exponential decay of transitions ${}^1\text{D}_2 \rightarrow {}^3\text{F}_4$, ${}^1\text{D}_2 \rightarrow {}^3\text{H}_6$ and ${}^3\text{H}_4 \rightarrow {}^3\text{H}_6$, was studied using the Inokuti–Hirayama procedure [65, 66]. The results indicate a dominant dipole–dipole interaction between Tm^{3+} ions. The data allowed us to determine the critical radius for different concentrations as shown in Table 7. A comparison of the critical radius with the average distance between ions suggests the presence of Tm^{3+} clusters in the samples. Formation of clusters may contribute to increase the UPC efficiency of the samples but it may be detrimental for operation of lasers. On the other hand, clusters may also favor

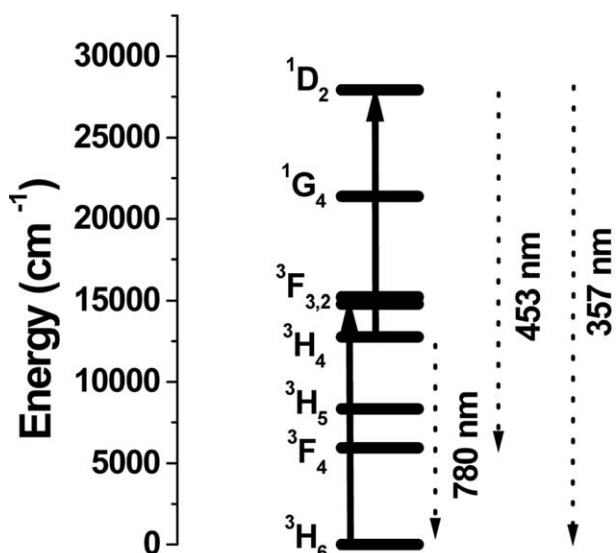


Fig. 5. Simplified energy-level scheme of Tm^{3+} . Solid lines represent the laser-induced transitions at 650 nm and the dashed lines correspond to the emissions indicated in Fig. 4.

Table 7. Comparison between critical radius (R_c) and mean distance (R_m) between Tm^{3+} ions as determined through observation of the fluorescence decay from ${}^1\text{D}_2$ level

Sample	Peak emission (cm^{-1})	R_c (Å)	R_m (Å)
Tm10	22 222	17	21
Tm20	22 222	17	17
Tm30	22 222	17	15
Tm10	27 550	17	21
Tm20	27 550	18	17
Tm30	27 550	18	15

radiation quenching, which is not of interest in general. Of course, further improvements in the preparation techniques have to be introduced to have control of clustering formation for particular applications.

4.1.3. $\text{Pr}^{3+}/\text{Nd}^{3+}$ -codoped FIG

UPC processes involving pairs of Pr^{3+} or pairs of Nd^{3+} were reported in the past. For instance, in crystals doped with Pr^{3+} , it was identified a process where two Pr^{3+} ions in the excited state ${}^1\text{D}_2$ exchange energy in such way that one of the ions decays nonradiatively to the ground state, while the other one is promoted to multiplet (${}^3\text{P}_1$, ${}^1\text{I}_6$). Emission at 480 nm due to transition ${}^3\text{P}_0 \rightarrow {}^3\text{H}_4$ and a weak emission at 470 nm due to transition (${}^3\text{P}_1$, ${}^1\text{I}_6$) $\rightarrow {}^3\text{H}_4$ were observed [67–69]. In glasses this effect was originally reported in [70] and later in [31, 71]. Processes involving pairs of Nd^{3+} ions that exchange energy were studied in crystals [72, 73] and, recently, similar processes were observed in FIG [34, 74–77], where efficient UPC emission was detected. Experiments were also reported involving triads $\text{Nd}^{3+}\text{--Pr}^{3+}\text{--Pr}^{3+}$ in LaF_3 [78] and UPC due to triads of Pr^{3+} was observed in $\text{LaF}_3:\text{Pr}^{3+}$ [79, 80]. More recently, UPC due to Nd^{3+} triads was investigated in crystals [81] and in fluoroindate glasses [35].

In this section we discuss evidences of ET processes involving triads and quartets of $\text{Nd}^{3+}/\text{Pr}^{3+}$ ions.

The absorption spectrum of the sample Pr_2Nd_2 in the visible range is shown in Fig. 1c. The broad features can be identified with transitions originating from the Pr^{3+} ground state (${}^3\text{H}_4$) and from the Nd^{3+} ground state (${}^4\text{I}_{9/2}$). The spectrum obtained for the sample Pr_2Nd_1 is similar, with no changes in the wavelengths of maximum absorption. All transitions are inhomogeneously broadened and the bands intensities are dependent on the ions concentrations. The spectrum of the sample without Nd^{3+} , but with 0.2% of Pr^{3+} , was previously reported [31].

The emission spectrum for excitation at 588 nm is shown in Fig. 6 for the sample with Pr_2Nd_1 . The four bands located from 350 to 460 nm are due to Nd^{3+} transitions, and the peaks at 470 and 480 nm are due

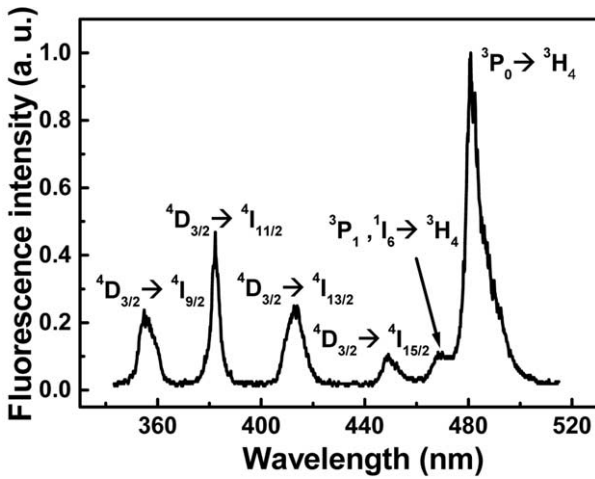


Fig. 6. Emission spectrum of sample Pr2Nd1 for excitation at 588 nm.

to Pr³⁺ ions. The states involved in the transitions are indicated in Fig. 6.

To characterize the UPC pathways, the intensity of each fluorescence band was measured as a function of the laser intensity. The signals present a quadratic dependence with the laser intensity, which indicates that two laser photons are required to generate each UPC photon emitted. Time-resolved fluorescence measurements were also performed varying the wavelength of the pump dye laser between 577 and 588 nm.

With basis on the signal behavior as a function of the laser intensity, we first investigate the possibility that the fluorescence emission at ~470 nm and ~480 nm could be produced via the process reported in [67–69]. However, although ET between two Pr³⁺ ions may be involved in the process that enables emission at 480 and 470 nm, the presence of Nd³⁺ plays an important role in the process. This was verified comparing the UPC efficiency of the Nd³⁺/Pr³⁺-codoped samples with the efficiency of a sample with 0.2% of Pr³⁺ only. An enhancement of the UPC intensity at 480 nm and at 470 nm, by two orders of magnitude with respect to a sample without Nd³⁺, was observed in the codoped samples. This is understood considering that: (i) the presence of Nd³⁺ increases the number of possible excitation pathways; (ii) the oscillator strength of the ⁴I_{9/2}→(²G_{7/2}+⁴G_{5/2}) transition in Nd³⁺ is, approximately, five times larger than for transition ³H₄→¹D₂ in Pr³⁺, and (iii) because of the large ET efficiency between Nd³⁺ and Pr³⁺ ions [78, 81, 82]. Thus, the emission at 480 nm and 470 nm may be due to processes that involve pairs (Pr–Pr), triads (Nd–Pr–Pr) or quartets (Nd–Pr–Pr–Nd). The last two process are more probable because of the enhancement factor of ~100 observed in the samples containing both Nd³⁺ and Pr³⁺. We expect

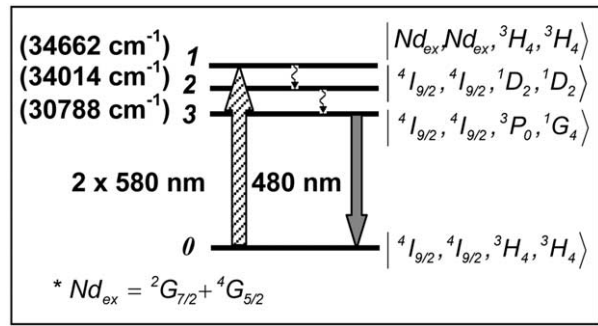


Fig. 7. Upconversion pathways for the Nd³⁺–Pr³⁺ quartets.

that the absorption of laser photons occur mainly through Nd³⁺ ions, which resonantly transfer their energy to the Pr³⁺ ions in their neighborhood. ET from Nd³⁺ at (²G_{7/2}+⁴G_{5/2}) states to Pr³⁺ is a resonant process where the acceptors make transition ³H₄→¹D₂, while the donor Nd³⁺ ion decays to the ground state. Following this step, two Pr³⁺ acceptors in state ¹D₂ exchange energy and one of them is promoted to the multiplet (³P_J, ¹I₆). The other ion decays to the ground state. Finally emission corresponding to ³P₀→³H₄ at 480 nm is observed. Fig. 7 illustrates the UPC process in the quartet case with the relevant states written, in a first approximation, as a direct product of the ions states. The triad and dyad cases can be represented in an analogous way. The rate equations for the density of populations, n_i ($i = 1, 2, 3$), in the quartets levels can be written as:

$$dn_1/dt = \sigma_0 \Phi \cdot n_0 - W_{12} \cdot n_1 - \gamma_1 \cdot n_1 \quad (11)$$

$$dn_2/dt = W_{12} \cdot n_1 - W_{23} \cdot n_2 - \gamma_2 \cdot n_2 \quad (12)$$

$$dn_3/dt = W_{23} \cdot n_2 - \gamma_3 \cdot n_3 \quad (13)$$

where Φ is the photon flux, σ_0 is the absorption cross-section, W_{nm} is the ET rate from state $|n\rangle$ to state $|m\rangle$, and γ_n is the relaxation of state $|n\rangle$ due to all possible mechanisms, except decay to state $|2\rangle$ or $|3\rangle$.

The system of equations (11)–(13) has the following solution for $t > \tau$, where τ is the laser-pulse duration.

$$\begin{cases} n_2(t) = n_2(\tau) \cdot e^{-(W_{23} + \gamma_2) \cdot t} & (14) \\ n_3(t) = \frac{n_2(\tau) \cdot W_{23}}{(W_{23} + \gamma_2) - \gamma_3} \cdot [e^{-\gamma_3 \cdot t} - e^{-(W_{23} + \gamma_2) \cdot t}] & (15) \end{cases}$$

Fig. 8 shows the fluorescence temporal profile for the sample Pr2Nd1 where the solid line represents a fitting of the $n_3(t)$ function, as given in equation (15). The numerical fitting gives a reasonable set of parameters, where it is possible to identify the ³P₀ lifetime, $(\gamma_3^{-1}) \sim 14 \mu\text{s}$, and the ¹D₂ lifetime, $(W_{23} + \gamma_2)^{-1} \sim 106 \mu\text{s}$. Unfortunately, it was not pos-

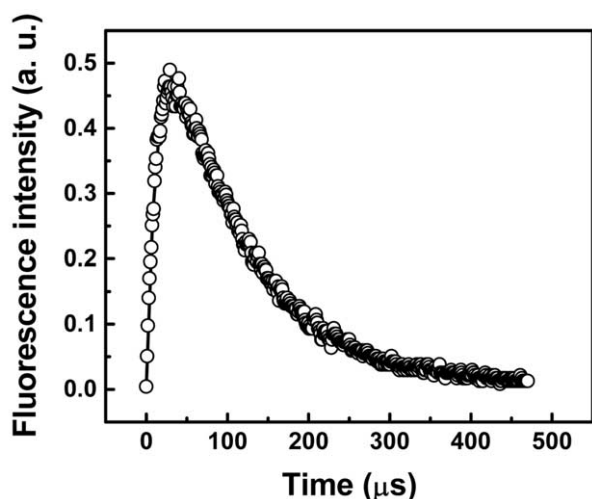


Fig. 8. Fluorescence temporal evolution at 480 nm for sample Pr₂Nd₁ pumped at 588 nm.

sible to obtain a value for the ET rate from Nd³⁺ to Pr³⁺, because the nonradiative transition rate between levels 1 and 2 is very large due to the small energy gap of $\sim 650\text{ cm}^{-1}$ between the two levels. Also it is impossible to determine unambiguously the main UPC mechanism (due to triads or quartets) via the temporal fluorescence analysis, because the estimated differences in the time evolution for triads or quartets is less than 1 ns, which is below the resolution of our data acquisition system. Moreover, it is not possible to infer, on the basis of the statistical distribution of ions, which contribution is more important, because, although the number of quartets would be smaller than the number of triads for a homogeneous distribution of RE ions, the probability of quartets excitation is at least five times larger than for the triads. Clustering of RE ions is another possibility that makes the analysis more difficult. All these points will be investigated in further work.

4.2. Multiphonon-assisted UPC

4.2.1. Nd³⁺ doped FIG

The study of multiphonon (MP) assisted processes in RE-doped materials has been a subject of large interest. In the past, luminescence and UPC mediated by phonons have been analyzed by Auzel et al. [83–86]. They demonstrated that it is possible to induce luminescence in solids doped with RE ions, even when the difference between the excitation frequency and the electronic-transition frequency is larger than the maximum phonon frequency of the host material. This was observed both for transitions involving creation or annihilation of phonons. Furthermore, contrary to what was generally thought, Auzel et al. [83–86] showed that MP-assisted processes

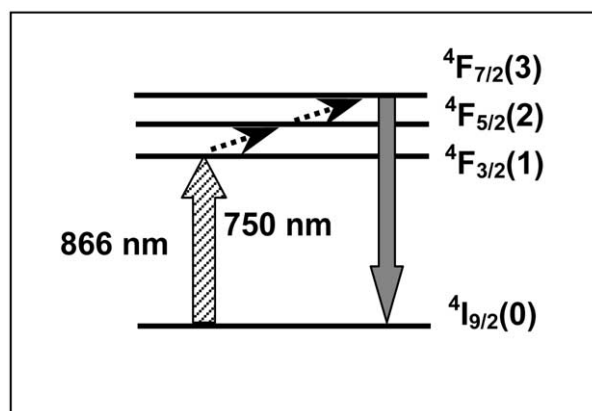


Fig. 9. Simplified energy-level scheme of Nd³⁺ ion, representing the pathway for emission at 750 nm when pumping at 866 nm.

should be described in terms of an ‘effective phonon mode’ – EPM (or ‘promoting mode’), with a frequency smaller than the phonon cut-off frequency of the host material. Recently, it was demonstrated that besides the scientific interest, studies of phonon-assisted processes are useful to photonic applications such as phase conjugation [87], lasers [88], avalanche UPC [89] and laser cooling of solids [90].

In this section, we show that UPC processes assisted by MP absorption can be highly efficient if optical transitions and thermal coupling between electronic levels are conveniently exploited. Our studies were mainly concentrated in the investigation of MP assisted UPC process from 866 nm to 750 nm. A forty-fold enhancement of the UPC emission intensity was observed when the temperature of the sample was varied from 298 to 498 K.

The absorption spectrum of a Nd-doped sample is shown in Fig. 1d.

The upconverted fluorescence spectrum was observed with several emission bands located from 350 to 750 nm. They are mainly due to UPC processes involving ET between two and three Nd³⁺ ions. These processes were studied previously in Ref. [34, 35, 75–77]. However, the line centered at 750 nm presents a linear dependence with the laser power and it was assigned as a transition from level $^4F_{7/2}$ to the ground state. It originates through a process where one laser photon is absorbed to level $^4F_{3/2}$, followed by successive absorption of phonons to $^4F_{7/2}$ via the thermally coupled excited state $^4F_{5/2}$, as indicated in Fig. 9.

We monitored the integrated fluorescence emission at 750 nm as a function of the sample temperature, while the laser intensity was kept constant at 160 mW. The data obtained are presented in Fig. 10, which shows a signal increase when the temperature is varied from 298 to 498 K. The solid line in the figure

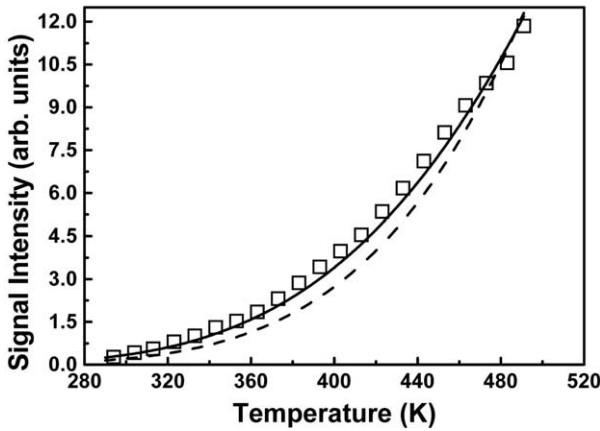


Fig. 10. Temperature dependence of the emission centered at 750 nm. Solid (dashed) line represents equation (19) with effective phonon mode of 310 cm^{-1} (maximum phonon energy of 507 cm^{-1}).

represents theoretical results which are obtained considering the subset of energy levels corresponding to $^4\text{I}_{9/2}$ (level 0); $^4\text{F}_{3/2}$ (level 1); $^4\text{F}_{5/2}$ (level 2), $^4\text{F}_{7/2}$ (level 3) and $^2\text{P}_{1/2}$, $^2\text{D}_{5/2}$ (level 4) and following the approach described below. A rate equation system written for the population densities n_i ($i = 1, 2, 3$) assumes the form:

$$dn_1/dt = \sigma_0 \Phi n_0 - A_{12}(T) n_1 - \gamma_1(T) n_1 - \sigma_1(T) \Phi n_1 \quad (16)$$

$$dn_2/dt = A_{12}(T) n_1 - A_{23}(T) n_2 - \gamma_2(T) n_2 \quad (17)$$

$$dn_3/dt = A_{23}(T) n_2 - \gamma_3(T) n_3 \quad (18)$$

where Φ is the photon flux, σ_0 is the absorption cross-section corresponding to transition $^4\text{I}_{9/2} \rightarrow ^4\text{F}_{3/2}$ ($5.0 \times 10^{-20} \text{ cm}^2$) and $\sigma_1(T)$ is the phonon-assisted one-photon absorption cross-section between states 1 and 4, from which other transitions occur contributing to UPC emissions. The absorption cross-sections for excited state transitions from levels $^4\text{F}_{5/2}$ ($\sigma_2(T)$) and $^4\text{F}_{7/2}$ ($\sigma_3(T)$) to higher lying levels were not included in our model, since their resonant parts, calculated on the basis on JO theory, have values that are considerably less than the resonant part of $\sigma_1(T)$, which is equal to $\sigma_1^0 = 1.5 \times 10^{-22} \text{ cm}^2$. The MP rates are given by $A_{ij}(T) = C_{ij}^{\text{ep}} P_{ij}(T)$, where C_{ij}^{ep} is proportional to the electron-phonon coupling strength and $P_{ij}(T)$ represents the phonon occupancy number given by $P_{ij}(T) = (\exp(\hbar \omega/k T) - 1)^{-q_{ij}}$, where q_{ij} is the number of phonons with energy $\hbar \omega$ involved in the MP excitation from level i to level j , k is the Boltzmann constant and T is the absolute temperature of the sample. The temperature-dependent absorption cross-section is given by $\sigma_1(T) = \sigma_1^0 [\exp(\hbar \omega/k T) - 1]^{-q}$, where the exponent q accounts for the number of effective phonons participating in the absorption process. The population relaxation rates are given by

$\gamma_i(T) = \gamma_i^{\text{rad}} + W_i^{\text{NR}}(T)$, with $(\gamma_i^{\text{rad}})^{-1}$ the radiative decay time. $W_i^{\text{NR}}(T)$ is the nonradiative relaxation rate from level i due to MP relaxation processes.

The steady-state population of $^4\text{F}_{7/2}$ level can be found solving equations (16)–(18) and is given by:

$$n_3(T) = \frac{\sigma_0 \Phi A_{12}(T) A_{23}(T) n_0}{\gamma_3(T) [A_{12}(T) + \gamma_1(T) + \sigma_1(T) \Phi] \cdot [A_{23}(T) + \gamma_2(T)]} \quad (19)$$

The signal intensity shown in Fig. 9 is proportional to $n_3(T)$. Thus, in order to compare equation (19) with the data of Fig. 10, the following procedure was used. To determine $n_3(T)$, a reference temperature ($T_0 = 300 \text{ K}$) was chosen and $W_i^{\text{NR}}(T)$ was determined through the following expression obtained from [91, 92]:

$$W_i^{\text{NR}}(T) = W_i^{\text{NR}}(T_0) \left[\frac{1 - \exp(-\hbar \omega/k T)}{1 - \exp(-\hbar \omega/k T_0)} \right]^{-q_i} \quad (20)$$

where q_i represents the number of effective phonons involved in the relaxation of level i to the closest low-energy level. The other relaxation parameters in equation (19) were obtained using the measured lifetimes of states $^4\text{F}_{3/2}$ ($\sim 186 \mu\text{s}$), $^4\text{F}_{5/2}$ ($\sim 5 \mu\text{s}$) and $^4\text{F}_{7/2}$ ($\sim 47 \mu\text{s}$) at room temperature [93], as well as their nonradiative emission rates, $W_i^{\text{NR}}(T_0)$, determined through the energy-gap law [94, 95] as 0.5 Hz, $1 \times 10^8 \text{ Hz}$ and $1.5 \times 10^8 \text{ Hz}$, respectively.

The comparison of equation (19) to the experimental results shown in Fig. 10 was made and the best agreement is observed when EPM are assumed to participate in all MP processes, as proposed in [83–86]. The parameters obtained from the fitting were $q = 1$, $q_{12} = q_{23} = 3$ and $\omega = 310 \text{ cm}^{-1}$. Also shown in Fig. 10 is a curve (dashed line) obtained from equation (19) for $\omega = 507 \text{ cm}^{-1}$ which is the energy of the most energetic phonons in the FIG matrix [7]. The mismatch of the dashed line with the experimental points obviates that the most energetic phonons do not dominate the MP absorption processes. In fact, several phonon modes contribute in a way that is determined by the phonon distribution density of states (PDDS) and the description in terms of EPM represents a kind of statistical average, which takes into account the characteristics of the PDDS. The value of $\omega = 310 \text{ cm}^{-1}$ obtained from equation (19) corresponds to the EPM frequency of the glassy matrix. A comparison of this result with the results of [83] for ZBLAN glass (phonon cut-off frequency: $\sim 580 \text{ cm}^{-1}$, EPM frequency: 325 cm^{-1}) indicates a similar energy dependence of the PDDS in both materials.

The results presented above, together with the previous ones reported in [91, 92], provide indication that the exploitation of MP processes may increase the efficiency of RE-doped systems for particular applications. On the basis of the results above as well as those of [91, 92], we believe that further exploitation of MP processes may improve the performance of RE-doped upconverters. Of course, in all cases, one must work in temperatures far below the onset of crystallization of the sample.

4.2.2. $\text{Yb}^{3+}/\text{Tb}^{3+}$ -codoped FIG

In this section, we report the observation of multiphonon-assisted cooperative energy transfer (MACET) between rare-earth ions in FIG. Bright UPC fluorescence from Tb^{3+} ions is observed due to MACET from Yb^{3+} ions excited using an infrared diode laser. This is a new effect reported here for the first time.

The absorption spectrum of a $\text{Yb}^{3+}/\text{Tb}^{3+}$ sample is shown in Fig. 1e.

Fig. 11 shows a typical UPC fluorescence spectrum for excitation at 1064 nm, whose frequency is $\sim 820 \text{ cm}^{-1}$, i.e. below the ${}^2\text{F}_{7/2} \rightarrow {}^2\text{F}_{5/2}$ resonance of Yb^{3+} ions. The UPC emissions observed are due to Tb^{3+} ions and the corresponding transitions are indicated in the figure. The intensity dependence of the lines at $\sim 414 \text{ nm}$ and $\sim 545 \text{ nm}$ were determined as a function of the laser intensity and showed cubic and quadratic behavior respectively, indicating that three and two laser photons are involved in the UPC processes. The emissions at 545 nm are explained considering that initially Yb^{3+} ions are excited to the ${}^2\text{F}_{5/2}$ state by the pump laser with the simultaneous absorption of phonons. Then, cooperative energy transfer between a pair of excited Yb^{3+} ions and a neighbor Tb^{3+} ion in the ground state occurs. Therefore, the Tb^{3+} ion is promoted to state ${}^5\text{D}_4$ and afterwards green fluorescence is emitted.

The blue emission at $\sim 414 \text{ nm}$ also originates from the same MACET process, but after excitation to ${}^5\text{D}_4$, a laser photon is absorbed promoting the Tb^{3+} ion to state ${}^5\text{D}_1$, or a neighbor level, which decays later to ${}^5\text{D}_3$ and ${}^5\text{G}_6$. Finally, radiative emissions from ${}^5\text{D}_3$ and ${}^5\text{D}_6$ to lower Tb^{3+} energy levels take place. The UPC pathways are illustrated in Fig. 12, which exhibits a simplified level scheme of the interacting atoms.

The solid lines indicate the laser excitation and the dotted lines represent the multiphonon absorption process. The dashed lines represent the cooperative energy transfer process. We observed that the blue and green UPC intensity was increased by a factor of ~ 55 when the temperature was varied from 300 to 530 K. A detailed study of this UPC process will be published elsewhere.

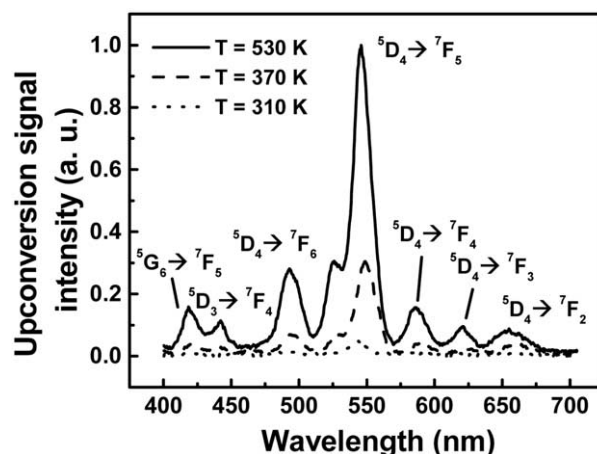


Fig. 11. Upconversion spectrum of sample Yb15Tb5 for excitation at 1064 nm.

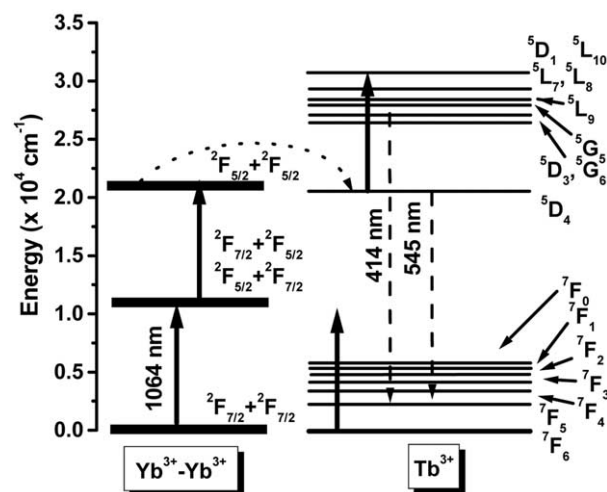


Fig. 12. Illustration of the frequency-upconversion pathways involving triads $\text{Yb}^{3+}\text{-Yb}^{3+}\text{-Tb}^{3+}$.

5. Conclusions

In summary, we presented some optical properties of fluoroindate glasses doped with Ho^{3+} , Tm^{3+} , Nd^{3+} and codoped with $\text{Pr}^{3+}/\text{Nd}^{3+}$ and $\text{Yb}^{3+}/\text{Tb}^{3+}$ ions. Upconversion processes were discussed with emphasis on the fluorescence dynamics and thermal behavior. The results show that fluoroindate glasses have a large potential for applications in photonics due to its mechanical and optical properties. Up to the present time most of the work was performed with bulk samples; however, we expect that further studies using FIG based fibers and optical waveguides may allow the operation of efficient and compact upconverters and amplifiers.

Acknowledgements. We would like to recognize the contributions of our colleagues and former graduate students, particularly L.E.E. de Araujo, W. Lozano, A.S. Gouveia Neto, J.R. Rios Leite, A.S.L. Gomes, L.H. Acioli and E.M. Pacheco. The financial support from Programa Nacional de Núcleos de Excelência – PRONEX/MCT (Brazil) is acknowledged.

References

- [1] M. Poulain, M. Poulain, G. Maze, French Patent No. 2 478 618, 1980.
- [2] J.P. Miranday, C. Jacoboni, R. Pope, US Patent No. 4 328 318, 1980.
- [3] G. Zhang, J.M. Jiang, M. Poulain, A.S. Delben, J.R. Delben, *J. Non-Cryst. Solids* 257 (1999) 135.
- [4] R.P. de Melo Jr, B.J.P. da Silva, E.L. Falcão-Filho, E.F. da Silva, D.V. Petrov, C.B. de Araújo, *Appl. Phys. Lett.* 67 (1995) 886.
- [5] M. Poulain, M. Poulain, H.H. Quenec, M.P. Glemont, Y. Messaddeq, C.B. de Araújo, French Patent No. 2 776 079, 1999.
- [6] G. Rault, J.L. Adam, F. Smektala, J. Lucas, *J. Fluorine Chem.* 110 (2001) 165.
- [7] R.M. de Almeida, J.C. Pereira, Y. Messaddeq, M.A. Aegerter, *J. Non-Cryst. Solids* 161 (1993) 105.
- [8] Y. Messaddeq, A. Delben, M. Boscolo, M.A. Aegerter, A. Soufiane, M. Poulain, *J. Non-Cryst. Solids* 161 (1993) 210.
- [9] V. Masteraro, S. Ribeiro, Y. Messaddeq, M.A. Aegerter, *J. Mater. Sci.* 31 (1996) 3441.
- [10] K. Annapurua, M. Hanumanthu, S. Buddhuhu, *Spectrochim. Acta* 48 A (1992) 791.
- [11] C.B. de Araújo, A.S.L. Gomes, L.H. Acioli, L. de S. Menezes, L.E.E. de Araujo, Y. Messaddeq, M.A. Aegerter, in: R.A. Brown (Ed.), *Trends in Chemical Physics*, Vol. 2, Research Trends, India, 1996, p. 59.
- [12] Y. Messaddeq, A. Delben, M.A. Aegerter, A. Soufiane, M. Poulain, *J. Mater. Res.* 8 (1993) 885.
- [13] A. Boutarfaia, M. Poulain, *J. Mater. Chem.* 10 (2000) 937.
- [14] P.P. Fedorov, R.M. Zakalyukin, L.N. Ignat'eva, V.M. Bouznik, *Russ. Chem. Rev.* 69 (2000) 705.
- [15] S. Todoroki, K. Hirao, N. Soga, *J. Non-Cryst. Solids* 143 (1992) 46.
- [16] B.J. Costa, M. Poulain, Y. Messaddeq, *Glass Sci. Technol.* 73 (Suppl. C1) (2000) 406.
- [17] A. Boutarfaia, M. Poulain, *Solid State Ionics* 144 (2001) 117.
- [18] A.A. Andrade, T. Catunda, R. Lebullenger, A.C. Hernandez, M.L. Baesso, *J. Non-Cryst. Solids* 284 (2001) 255.
- [19] A.A. Andrade, T. Catunda, R. Lebullenger, A.C. Hernandez, M.L. Baesso, *J. Non-Cryst. Solids* 273 (2000) 257.
- [20] R. Reiche, L.A.O. Nunes, C.C. Carvalho, Y. Messaddeq, M.A. Aegerter, *Solid State Commun.* 85 (1993) 773.
- [21] I.R. Martin, V.D. Rodriguez, Y. Guyot, S. Guy, G. Boulon, M.-F. Joubert, *J. Phys.: Condens. Mat.* 12 (2000) 1507.
- [22] C.T.M. Ribeiro, A.R. Zanatta, L.A.O. Nunes, Y. Messaddeq, M.A. Aegerter, *J. Appl. Phys.* 83 (1998) 2256.
- [23] S. Kishimoto, K. Hirao, *J. Appl. Phys.* 80 (1996) 1965.
- [24] W. Seeber, E.A. Downing, L. Hesselink, M.M. Fejer, D. Ehrt, *J. Non-Cryst. Solids* 189 (1995) 218.
- [25] M. Dejenka, E. Snitzer, R.E. Riman, *J. Lumin.* 65 (1995) 227.
- [26] T. Catunda, L.A.O. Nunes, A. Florez, Y. Messaddeq, M.A. Aegerter, *Phys. Rev. B* 53 (1996) 6065.
- [27] R. Rolli, S. Ronchin, M. Montagna, E. Moser, C. Duverger, V.K. Tikhomirov, A. Jha, M. Ferrari, *J. Non-Cryst. Solids* 280 (2001) 269.
- [28] I.R. Martin, V.D. Rodriguez, Y. Guyot, Y. Guy, G. Boulon, M.-F. Joubert, *J. Phys.: Condens. Mat.* 12 (2000) 1507.
- [29] I.R. Martin, V.D. Rodriguez, V. Lavin, U.R. Rodriguez-Mendoza, *J. Appl. Phys.* 86 (1999) 935.
- [30] I.R. Martin, P. Velez, V.D. Rodriguez, U.R. Rodriguez-Mendoza, V. Lavin, *Spectrochim. Acta A* 55 (1999) 935.
- [31] L.E.E. de Araújo, A.S.L. Gomes, C.B. de Araújo, Y. Messaddeq, A. Florez, M.A. Aegerter, *Phys. Rev. B* 50 (1994) 16219.
- [32] C.B. de Araújo, L. de S. Menezes, G.S. Maciel, L.H. Acioli, A.S.L. Gomes, Y. Messaddeq, A. Florez, M.A. Aegerter, *Appl. Phys. Lett.* 68 (1996) 602.
- [33] G.S. Maciel, C.B. de Araújo, Y. Messaddeq, M.A. Aegerter, *Phys. Rev. B* 55 (1997) 6335.
- [34] L. de S. Menezes, C.B. de Araújo, Y. Messaddeq, M.A. Aegerter, *J. Non-Cryst. Solids* 256 (1997) 213–214.
- [35] L. de S. Menezes, C.B. de Araújo, G.S. Maciel, Y. Messaddeq, M.A. Aegerter, *Appl. Phys. Lett.* 70 (1997) 683.
- [36] N. Rakov, G.S. Maciel, C.B. de Araújo, Y. Messaddeq, *J. Appl. Phys.* 91 (2002) 1272.
- [37] W. Lozano, C.B. de Araújo, C. Egalon, A.S.L. Gomes, B.J. Costa, Y. Messaddeq, *Opt. Commun.* 153 (1998) 271.
- [38] E. Martins, C.B. de Araújo, J.R. Delben, A.S.L. Gomes, B.J. da Costa, Y. Messaddeq, *Opt. Commun.* 158 (1998) 61.
- [39] G.S. Maciel, L. de S. Menezes, C.B. de Araújo, Y. Messaddeq, *J. Appl. Phys.* 85 (1999) 6782.
- [40] G.S. Maciel, L. de S. Menezes, A.S.L. Gomes, C.B. de Araújo, Y. Messaddeq, A. Florez, M.A. Aegerter, *IEEE Photon. Technol. Lett.* 7 (1995) 1474.
- [41] G.S. Maciel, N. Rakov, C.B. de Araújo, Y. Messaddeq, *J. Opt. Soc. Am. B* 16 (1999) 1995.
- [42] J. Fernández, R. Balda, M.A. Arriandaga, *Opt. Mater.* 4 (1994) 91.
- [43] J. Azkargota, I. Iparraguire, R. Balda, J. Fernández, E. Dénoue, J.L. Adam, *IEEE J. Quantum Electron.* 30 (1994) 1862.
- [44] M.J.F. Digonnet (Ed.), *Rare-Earth Doped Fiber Lasers and Amplifiers*, Marcel Dekker, New York, 1993.
- [45] R. Reisfeld, C.K. Jørgensen, *Lasers and Excited States of Rare-Earths*, Springer-Verlag, Germany, 1977.
- [46] B.R. Judd, *Phys. Rev.* 127 (1962) 750.
- [47] G.S. Ofelt, *J. Chem. Phys.* 37 (1962) 511.
- [48] D.S. Funk, S.B. Stevens, S.S. Wu, J.G. Eden, *IEEE J. Quantum Electron.* 32 (1996) 638.
- [49] R. Scheps, *Prog. Quantum Electron.* 20 (1996) 271.
- [50] B.R. Reddy, S. Nash-Stevenson, P. Venkateswarlu, *J. Opt. Soc. Am. B* 11 (1994) 923.
- [51] S. Kück, I. Sokólska, *Chem. Phys. Lett.* 325 (2000) 257.
- [52] S.A. Payne, J.A. Caird, L.L. Chase, L.K. Smith, N.D. Nielsen, W.F. Krupke, *J. Opt. Soc. Am. B* 8 (1991) 726.
- [53] M. Malinowski, R. Piramidowicz, Z. Frukacz, G. Chadeyron, R. Mahiou, M.F. Joubert, *Opt. Mater.* 12 (1999) 409.
- [54] M. Yamane, Y. Asahara, *Glasses for Photonics*, Cambridge University Press, Cambridge, UK, 2000.
- [55] J.Y. Allain, M. Monerie, H. Poignant, *Electron. Lett.* 26 (1990) 166.
- [56] D.C. Yeh, R.R. Petrin, W.A. Sibley, V. Madigou, J.-L. Adam, M.-J. Suscavage, *Phys. Rev. B* 39 (1989) 80.
- [57] W.J.L. Oomen, *J. Lumin.* 50 (1992) 317.
- [58] K. Hirao, S. Todoroki, N. Soga, *J. Non-Cryst. Solids* 143 (1992) 40.
- [59] L.B. Shaw, R.S.F. Chang, N. Djeu, *Phys. Rev. B* 50 (1994) 6609.
- [60] T. Hebert, R. Wannemacher, R.M. Mcfarlane, W. Lenth, *Appl. Phys. Lett.* 60 (1992) 2592.
- [61] H. Fujiwara, K. Sasaki, *J. Appl. Phys.* 86 (1999) 2385.
- [62] K. Mizato, D.F. de Sousa, A. Delben, J.R. Delben, S.L. de Oliveira, L.A.O. Nunes, *J. Non-Cryst. Solids* 273 (2000) 246.
- [63] A.S.L. Gomes, C.B. de Araújo, B.J. Ainslie, S.P. Craig-Ryan, *Appl. Phys. Lett.* 57 (1990) 2169.

- [64] C.B. de Araújo, A.S.L. Gomes, in: M.D. Levenson, E. Mazur, P.S. Pershan, Y.R. Shen (Eds.), *Resonances* (a volume in honor of the 70th birthday of Nicolaas Bloembergen), World Scientific, Singapore, 1991.
- [65] M. Inokuti, F. Hirayama, *J. Chem. Phys.* 43 (1965) 1978.
- [66] V. Jerez, C.B. de Araújo, Y. Messaddeq (to be published).
- [67] J.-C. Vial, R. Buisson, F. Madeore, M. Poirier, *J. Phys. (Paris)* 40 (1979) 913.
- [68] R. Buisson, J.-C. Vial, *J. Phys. (Paris)* 42 (1981) L115.
- [69] A. Lezama, M.S. Oriá, C.B. de Araújo, *Phys. Rev. B* 32 (1985) 7139.
- [70] E.M. Pacheco, C.B. de Araújo, *Chem. Phys. Lett.* 148 (1988) 334.
- [71] E.S. Moraes, M.M. Opalinska, A.S.L. Gomes, C.B. de Araújo, *Opt. Commun.* 84 (1991) 279.
- [72] N. Pelletier-Allard, R. Pelletier, *J. Lumin.* 46 (1990) 217.
- [73] R.B. Barthem, R. Buisson, F. Madèore, J.-C. Vial, J.-P. Chaminade, *J. Phys. (Paris)* 48 (1987) 379.
- [74] L.H. Acioli, J.T. Guo, C.B. de Araújo, Y. Messaddeq, M.A. Aegerter, *J. Lumin.* 72 (74) (1997) 68.
- [75] D.F. de Souza, F. Batalioto, M.J.V. Bell, S.L. Oliveira, L.A.O. Nunes, *J. Appl. Phys.* 90 (2001) 3308.
- [76] I.R. Mitchel, V.K. Bogdanov, P.M. Farrell, *Opt. Commun.* 155 (1998) 275.
- [77] J. Fernández, R. Balda, A. Mendioroz, M. Sanz, J.L. Adam, *J. Non-Cryst. Solids* 287 (2001) 437.
- [78] A. Lezama, *Phys. Rev. B* 34 (1986) 8850.
- [79] A. Lezama, M. Oriá, J.R. Rios Leite, C.B. de Araújo, *Phys. Rev. B* 32 (1985) 7139.
- [80] L.S. Lee, S.C. Rand, A.L. Schawlow, *Phys. Rev. B* 29 (1984) 6901.
- [81] A. Novo-Gradac, W.M. Dennis, A.J. Silversmith, S.M. Jacobsen, W.M. Yen, *J. Lumin.* 695 (1994) 60–61.
- [82] S.C. Goh, R. Pattie, C. Byrne, D. Coulson, *Appl. Phys. Lett.* 67 (1995) 768.
- [83] F. Auzel, Y.H. Chen, *J. Lumin.* 224 (1996) 66.
- [84] F. Pellé, F. Auzel, *J. Lumin.* 623 (1998) 76–77.
- [85] F. Auzel, *Phys. Rev. B* 13 (1976) 2809.
- [86] F. Auzel, F. Pellé, *Phys. Rev. B* 55 (1997) 11006.
- [87] H. Ni, S.C. Rand, *Opt. Lett.* 17 (1992) 1222.
- [88] P. Xie, T.R. Gosnell, *Opt. Lett.* 20 (1995) 1014.
- [89] M.-F. Joubert, *Opt. Mater.* 111 (1999) 981.
- [90] R.I. Epstein, M.I. Buchwald, B.C. Edwards, T.R. Gosnell, C.E. Mungan, *Nature (London)* 377 (1995) 500.
- [91] A.S. Oliveira, E.A. Gouveia, M.T. de Araujo, A.S. Gouveia Neto, C.B. de Araújo, Y. Messaddeq, *J. Appl. Phys.* 87 (2000) 4274.
- [92] E.A. Gouveia, M.T. de Araujo, A.S. Gouveia Neto, *Braz. J. Phys.* 31 (2001) 89.
- [93] L. de S. Menezes, MSci. Thesis, Universidade Federal de Pernambuco, Recife, Brazil, 1996 (in Portuguese).
- [94] M.J. Weber, *Phys. Rev.* 157 (1967) 262.
- [95] M.J. Weber, *Phys. Rev. B* 8 (1973) 54.